

# Rock Mass Characterization by High-Resolution Sonic and GSI Borehole Logging

F. Agliardi<sup>1</sup> · M. Sapigni<sup>2</sup> · G. B. Crosta<sup>1</sup>

Received: 1 December 2015 / Accepted: 8 June 2016 / Published online: 22 June 2016  
© Springer-Verlag Wien 2016

**Abstract** We investigate the relationships between the in situ P-wave velocity ( $V_p$ ) of rock masses, measured by borehole acoustic logging, and their Geological Strength Index (GSI), to support a reliable assessment of equivalent continuum rock mass properties at depth. We quantified both  $V_p$  and GSI in three deep boreholes drilled in a crystalline core complex of the central Italian Alps. The boreholes were driven up to 400 m in depth and provided high-quality drill cores in gneiss, schist and metasedimentary rocks with variable lithology. Geological and geomechanical logging was carried out for over 800 m of cores, and acoustic logging was performed for more than 600 m of borehole length. High-resolution core logging in terms of GSI was obtained using an original quantitative approach. Candidate empirical correlation functions linking  $V_p$  and GSI were tested by a two-step statistical analysis of the experimental dataset, including outlier removal and nonlinear regression analysis. We propose a sigmoid  $V_p$ –GSI equation valid over a depth range between 100 and 400 m. This accounts for extremely variable lithological, weathering and rock mass damage conditions, complementing existing shallow-depth approaches and showing potential for practical applications in different engineering settings.

**Keywords** Rock mass characterization · Acoustic logging · P-wave velocity · Geological Strength Index · Borehole geophysics · Empirical correlation

## 1 Introduction

A reliable assessment of the physical and mechanical properties of rock masses at depth is key to a number of geological, engineering and geohazard applications. Rock mass investigations usually exploit combinations of direct geomechanical core logging (Deere 1963; ISRM 1978; Bieniawski 1989; Cai et al. 2004; Palmstrom 2005) and indirect geophysical techniques (Sjøgren et al. 1979; McDowell 1993; Palmström 1995; Mavko et al. 1998; Barton 2007; King 2009). The geomechanical logging of high-quality borehole drill cores allows an accurate assessment of rock mass lithology and structure, individual discontinuity features (i.e., orientation, roughness, weathering) and rock mass fracture abundance (Dershowitz and Herda 1992), as well as direct estimates of rock mass quality indices (Barton et al. 1974; Bieniawski 1989; Palmström 1995; Hoek and Brown 1997). Nevertheless, the biased scanline character of boreholes, the limited investigated volumes and the extreme variability of rock mass features in complex lithological and structural conditions often limit the cost-effectiveness of rock mass characterization performed by direct investigations. These require an excessive number of expensive full-core boreholes to be drilled and logged to support large engineering projects. Therefore, considerable efforts were made in the last four decades to relate rock mass quality indices to physical properties measurable in the field by geophysical techniques, especially in reservoir exploration and tunneling applications (Hudson et al. 1980; Serra 1986; Griffiths and

✉ F. Agliardi  
federico.agliardi@unimib.it

<sup>1</sup> Department of Earth and Environmental Sciences, University of Milano-Bicocca, Piazza della Scienza 4, 20126 Milan, Italy

<sup>2</sup> Divisione Generazione ed Energy Management, ENEL Produzione S.p.A., Via Torino 16, 30172 Venezia-Mestre, Italy

King 1987; Barton 2007). The seismic P-wave velocity ( $V_p$ ) is the most used of these properties, which can be recorded up to great depth using different geophysical prospecting techniques (e.g., shallow seismic reflection or refraction, VSP, downhole, crosshole). It depends on a variety of factors including rock composition (Press 1966; Stacey 1977; Sjøgren 1984; Griffiths and King 1987), microcracking, density, porosity (Watkins et al. 1972; Nur et al. 1998), fabric and jointing anisotropy, and rock mass fracture intensity and alteration (Barton 2007 and references therein). After Deere et al. (1967), who related the seismic P-wave velocity (measured in the field and in the lab) to the rock quality designation (RQD), several authors attempted to find relationships between  $V_p$  and a number of rock mass quality estimators. Using an extensive shallow (<20 m) seismic refraction dataset, Sjøgren et al. (1979) and Palmström (1995) proposed relationships among  $V_p$ , RQD and linear fracture intensity (i.e., joints/m) for hard jointed crystalline rocks. King et al. (1978) related  $V_p$  measured by downhole acoustic logging and linear fracture intensity in boreholes. Barton (1991) proposed a relationship between  $V_p$  and the Q index (Barton et al. 1974) by correlating drill core logs and cross-hole datasets and suggested its use only at very shallow depth, because it neglects the effects of confining pressure at depth on  $V_p$  (Stacey 1977; New and West 1980). Cecil (1971) and Sjøgren et al. (1979) measured a strong increase in  $V_p$  with depth at very shallow levels (<100 m), with highest gradients in heavily jointed rocks. Barton (1995, 2002) proposed an empirical relationship relating  $V_p$ , Q and rock mass deformation modulus by accounting for the effects of depth and rock porosity. Nevertheless, at deeper levels (600–1200 m), Moos and Zoback (1983) found contrasting  $V_p$ -depth trends in different rock masses, including poorly variable  $V_p$  in rocks with few fractures,  $V_p$  increasing at depth in heavily jointed rocks and even  $V_p$ -depth gradient reversals in irregularly fractured rocks. The influence of fractures is larger at shallow levels due to acoustic aperture, which decreases with increasing confining stress (New and West 1980) and becomes negligible at depths of several hundreds of meters in jointed rocks (Westerman et al. 1982). Field  $V_p$  measurements have also been related to rock mass permeability and excavation damage zone (EDZ) characteristics (Sjøgren et al. 1979; Albert 2000; Barton 2007 and references therein).

Existing approaches to rock mass characterization by geophysical investigations mostly apply to hard crystalline rocks at shallow depths (upper few tens of meters), thus with limited practical applicability. Moreover, they rely on rock mass descriptors poorly suitable to describe the conditions of strongly deformed, weathered or damaged rocks characterized by small- to large-scale heterogeneity. Finally, empirical methods incorporating the effects of

confining pressure, fluid content and rock strength were generally poorly validated by in situ experimental data in complex geological conditions. Therefore, there is a need for: (1) versatile approaches to estimate rock mass quality descriptors suitable for varying geological conditions from drill cores; (2) statistically sound relationships between such descriptors and rock physical properties measured by geophysical methods.

In this perspective, we searched for correlations between the  $V_p$  measured by borehole acoustic logging (Brie et al. 1998; Franco et al. 2006; Haldorsen et al. 2006) and rock mass quality described in terms of the Geological Strength Index (GSI; Hoek et al. 1995, 2002). The latter is a descriptor of rock mass structure and weathering suitable for application to nearly all rock types and geological conditions. We quantified both  $V_p$  and GSI in three deep boreholes, drilled to support the initial design of a 9.2-km-long headrace tunnel in a crystalline core complex of the central Italian Alps (Fig. 1). The boreholes were driven up to 400 m in depth in gneiss and metasedimentary rocks (including gypsum–anhydrite, marbles, decomposed carbonates) and provided high-quality drill cores. In the same boreholes, more than 600 m of acoustic (sonic) logging was performed. We analyzed these datasets to: (1) carry out a high-resolution GSI logging of drill cores using an original quantitative approach; (2) derive empirical correlation functions linking GSI and  $V_p$  by statistical analysis.

## 2 Geological Setting

Investigated rocks belong to the Lepontine Alps, which include the deepest outcropping tectonic units of the Tertiary alpine orogen. They are made of crystalline basement nappes (Verampio, Antigorio and Monte Leone units; Fig. 1) interlayered with their metasedimentary Mesozoic cover sequences, referred to as “Teggiolo zone” and including the Baceno and Teggiolo metasediments, respectively (Milnes et al. 1981; Grasemann and Mancktelow 1993; Steck 2008; Steck et al. 2013; Fig. 1). This structural architecture (Figs. 1, 2) is the result of a multi-stage tectonic history in changing metamorphic and rheological conditions, accompanying thrusting of the nappe stack with crustal shortening of tens of kilometers, successive refolding and later tectonic exhumation along the Simplon Fault Zone (Mancktelow 1985; Maxelon and Mancktelow 2005; Campani et al. 2010).

The geological structure of the investigated portion of the Antigorio valley (i.e., the eastern flank of Mt. Cistella between Crodo to the S and Baceno to the N) is depicted in the N–S cross section of Fig. 2. At shallower depth, the main feature is represented by the thick Antigorio unit (ANT in Fig. 1), made of leucocratic biotite-rich

**Fig. 1** Simplified structural sketch of the Simplon dome (modified after Grasemann and Mancktelow 1993; Steck et al. 2013). VER Verampio basement, ANT Antigorio basement, ML Monte Leone basement. Gray areas Mesozoic metasedimentary units of the “Teggiolo zone” (Steck et al. 2013), subdivided into “Baceno metasediments” (*b*) and “Teggiolo metasediments” (*t*). Trace of the geological cross section in Fig. 2 is outlined

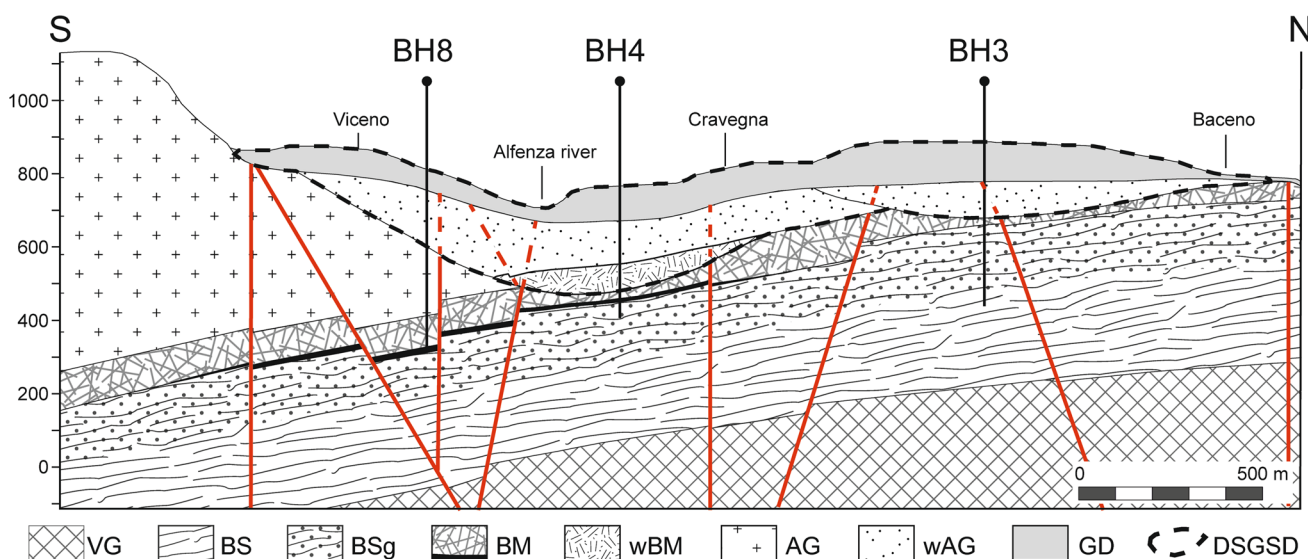
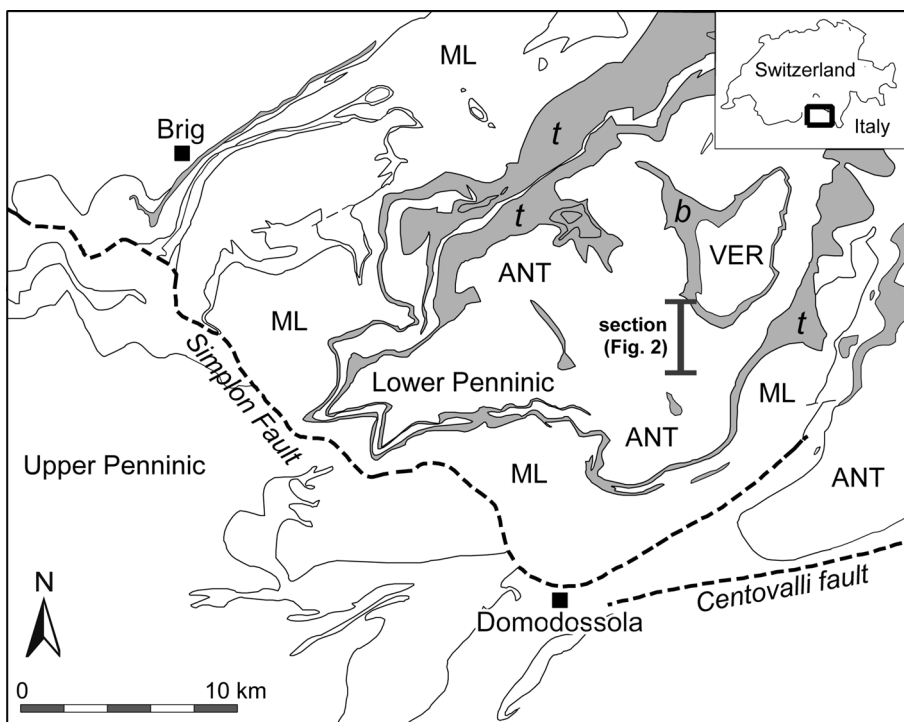


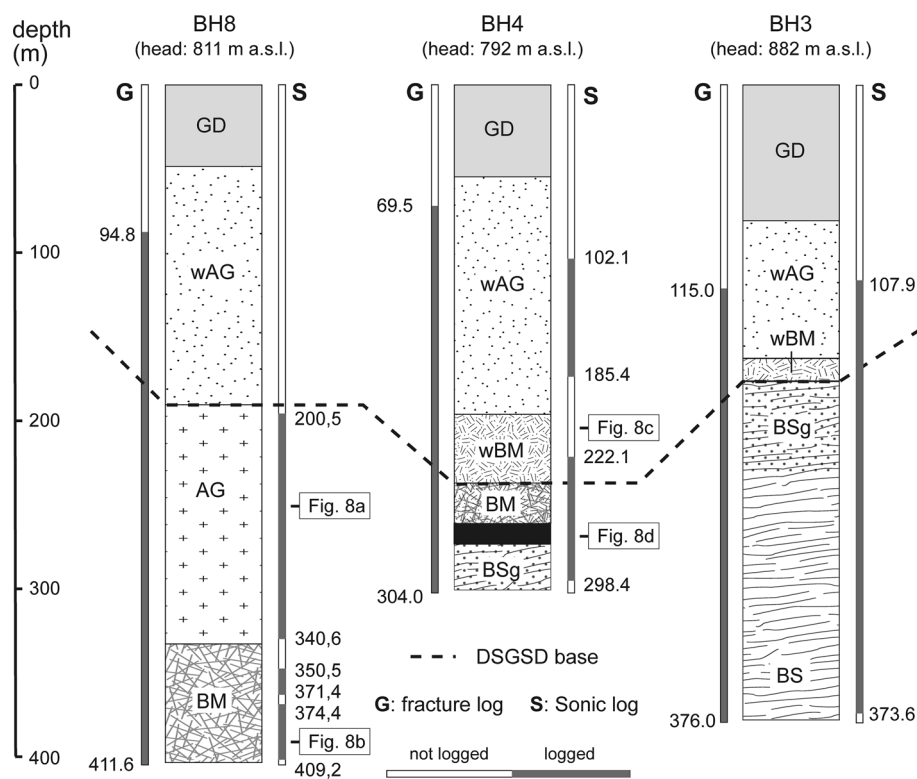
**Fig. 2** N-S geological cross section, passing through the studied boreholes on the right flank of the Antigorio valley (cross-sectional trace in Fig. 1). Keys to lithological units: VG Verampio granitic gneiss, BS Baceno mica schist, BSg garnet-rich Baceno mica schist, BM Baceno Mesozoic metasediments including gypsum–anhydrite,

sands, marbles and calc-schist (*black basal anhydrite layer*); *wBM* strongly fractured and weathered Baceno metasediments, AG Antigorio orthogneiss, *wAG* strongly fractured and weathered Antigorio orthogneiss, GD glacial deposits. *Red lines* faults. *Dashed line* boundary of DSGSD mass (color figure online)

orthogneiss (AG in Fig. 2) with low compositional and textural variability (Bigioggero et al. 1977). At depth, most of the studied domain belongs to the deeper Verampio basement unit (VER in Fig. 1), including late Variscan granitic gneiss (VG in Fig. 2) and its original host rock now represented by the Baceno mica schist (BS in Fig. 2),

which is rich in garnet in the upper 70–100 m (BSg). A thick multilayer of Mesozoic metasediments (Baceno metasediments, BM in Fig. 2) separates the two basement units. In the investigated area (Fig. 3), the BM have an average thickness of about 70 m and are characterized by highly variable lithology, including a basal gypsum–

**Fig. 3** Geological borehole logs. Keys to lithological units: *BS* Baceno mica schist, *BSg* garnet-rich Baceno mica schist, *BM* Baceno metasediments (*black* basal gypsum–anhydrite layer); *wBM* strongly fractured and weathered Baceno metasediments, *AG* Antigorio orthogneiss, *wAG* strongly fractured and weathered Antigorio orthogneiss, *GD* glacial deposits. Borehole segments with available fracture logs (G) and acoustic logs (S) are outlined, as well as the locations of example core units in Fig. 8. Horizontal distances between the boreholes are out of scale (BH8–BH4: 400 m; BH4–BH3: 1000 m)



anhydrite layer, at least two decomposed carbonate layers, dolomitic marbles and calc-schist. Between Viceno and Crodo reworked glacial deposits up to 80 m thick mantle the bedrock.

Detailed geological and geomorphological mapping, borehole logging and a geophysical survey (Sapigni et al. 2012) allowed identifying a large deep-seated gravitational slope deformation (DSGSD; Agliardi et al. 2001, 2012) in the northern part of the investigated area (Fig. 2). This is characterized by complex geometry and thickness ranging from 180 to 250 m. Below the thick glacial cover deposits, rock masses affected by DSGSD mainly consist of weak to very weak, strongly weathered to decomposed Antigorio gneiss (AGw in Fig. 2). At greater depth, the DSGSD also involves strongly altered Baceno metasedimentary rocks (BMw) resting above the unaffected basal gypsum–anhydrite layer.

### 3 Site Investigations

#### 3.1 Borehole Drilling and Characterization

Three 300–400 m deep boreholes (BH3, BH4 and BH8; Fig. 3) were drilled along a N–S alignment (Figs. 1, 2, 3). Coring was made using a standard 101-mm double-tube core barrel to depths of 100–110 m. At higher depth, wire

line HQ (96 mm) core barrels were used, except in the BH8 where the deepest 37 m were drilled using a NQ (75.7 mm) core barrel. A total length of 1092 m of high-quality drill cores was extracted, with core diameters ranging between 47.6 and 63.5 mm. For all of the three boreholes, the total core recovery (TCR) ranged between 80 and 100 %, with only few runs between 50 and 70 %. The average drilling rate was in the range 6–10 m/day.

Detailed geological core logging and geophysical investigation by acoustic logging (see Sect. 3.4) and borehole televiewer (BHTV) were carried out for most of the drilled depth (Fig. 3). Petrographic analyses by standard optical microscopy, scanning electron microscopy and X-ray diffraction were performed on a number of samples to characterize the borehole geology (rock types, meso- and microfabric, structural features). In addition, we carried out a standard geomechanical core logging on about 812 m of drill cores (Fig. 3). This included: (a) characterization of individual discontinuity properties (i.e., location, inclination, roughness—JRC, weathering/alteration, aperture, infilling; ISRM 1978); (b) evaluation of rock mass quality and fracture intensity descriptors, including total core recovery (TCR), rock quality designation (RQD; Deere 1963), fracture spacing and parameters related to the Barton Q-system (joint alteration number, Ja, joint roughness number, Jr, joint fracture number, Jn, JRC; Barton et al. 1974).

### 3.2 Borehole Stratigraphy

Site investigations allowed reconstructing the borehole stratigraphy in detail (Figs. 2, 3). In particular, the three boreholes crossed a top layer of glacial deposits made of gravelly silty sands with gneiss pebbles and boulders, with thickness ranging between 53 m (BH8) and 97 m (BH3). At greater depth, the boreholes entered biotite-rich orthogneiss belonging to the Antigorio unit. This occurs in two contrasting geomechanical facies: (a) an upper one made of intensely fractured and weathered rock and cataclastic breccia layers (wAG in Figs. 2, 3), characterized by RQD values mostly below 40–50 and by the scattered occurrence of RQD = 0 or high RQD layers, reflecting extreme heterogeneity; (b) a lower facies (AG) made of sound, unweathered and poorly fractured orthogneiss, well exposed in rock outcrops and quarries in the area. AG is characterized by RQD in the range 50–85, with interlayered weak layers (RQD < 30). X-ray diffraction analyses showed no significant differences in rock mineral composition between the two facies. wAG occurs in the rock volume affected by the DSGSD.

The Antigorio gneiss takes most of the BH8 log, due to the regional attitude of the nappe stack which steepens toward the South approaching the Simplon Fault zone (Fig. 2). Thus, the boundary between the Antigorio gneiss and the underlying Baceno metasediments (BM) occurs at different depths in the studied boreholes. In BH8, BM rocks are found at about 340 m in depth and are made of calcite and dolomite marbles, with minor volumes of calc-schist and mica schist (Fig. 3). A distinctive lithological and geomechanical feature of the BM sequence is the occurrence of two cohesionless carbonate layers (carbonate “sands”) with a grain size distribution in the range 1.0–0.1 mm. These layers are not genetically related to DSGSD, because they are found also at great depth in BH8 well below the DSGSD affected zone. The extreme lithological and geomechanical heterogeneity of the BM sequence is mirrored by highly scattered RDQ values, ranging between 0 and 40 in cohesionless and fractured layers, but reaching up to 75 in the stronger marble layers. In the borehole BH4, Baceno metasediments are found at

shallower depth and are partially involved in the DSGSD, where they appear strongly fractured and weathered (wBM) up to a depth of about 250 m. Below, the boreholes encountered sound dolomitic marbles with high RQD values and scattered fractured horizons, overlying a sound basal anhydrite layer (Fig. 3). A thinner slice of wBM also occurs at lower depth in BH3, at the DSGSD base. At greater depths, boreholes BH4 and BH3 enter the deepest structural unit, i.e., the Baceno mica schist (BS), characterized by an abundance (15–30 % in volume) of cm-size garnets in the upper 50–60 m (BSg). To the north, BS rocks are well represented in the BH3, where they are characterized by good geomechanical quality with RQD in the range 70–100.

### 3.3 Intact Rock Properties

Laboratory investigations were carried out on selected samples of orthogneiss (AG), dolomitic marble (BM), anhydrite (BM) and mica schist (BS). For each rock type, 30 specimens were prepared for standard uniaxial compression, triaxial compression and indirect tension (Brazilian) tests. Rock density and physical properties were determined (i.e., P-wave and S-wave velocity, dynamic moduli) according to ASTM D2845-08 (2008). A summary of intact rock properties, measured in dry laboratory conditions and unconfined compression, is reported in Table 1. These results provide reference values for comparison to in situ measurements and demonstrate a relatively weak rock type control on rock physical properties measured in boreholes, which mainly reflect fractured rock mass conditions.

### 3.4 Borehole Acoustic Logging

Acoustic (or sonic) logging is the recording of travel times of acoustic waves from one or more transmitters to receivers installed at suitable distances along a borehole probe. Acoustic logging techniques were developed since the 1960s (White 1962, 1967) with particular focus on the analysis of formation porosity (Serra 1986; Jorden and Campbell 1986; Brie et al. 1998; Franco et al. 2006;

**Table 1** Summary of laboratory measurements of intact rock properties for some studied rock types (unconfined conditions, loading and wave pulsing directions orthogonal to foliation)

	Unit weight (kN/m <sup>3</sup> )		V <sub>p</sub> (m/s)		V <sub>s</sub> (m/s)		UCS (MPa)		Et <sub>50</sub> (GPa)	
	Mean	COV	Mean	COV	Mean	COV	Mean	COV	Mean	COV
AG orthogneiss	27.0	0.02	4740	0.09	–	–	105.4	0.17	78.0	0.36
BM marble	27.1	0.01	4193	0.04	2606	0.06	105.6	0.06	32.0	0.05
BM anhydrite	29.2	0.02	4770	0.13	2431	0.09	22.7	0.17	30.9	0.17
BS mica schist	27.3	0.02	4606*	0.15*	–	–	114.9	0.43	109.0	0.27

COV coefficient of variation

\* Data after Gong (2005)

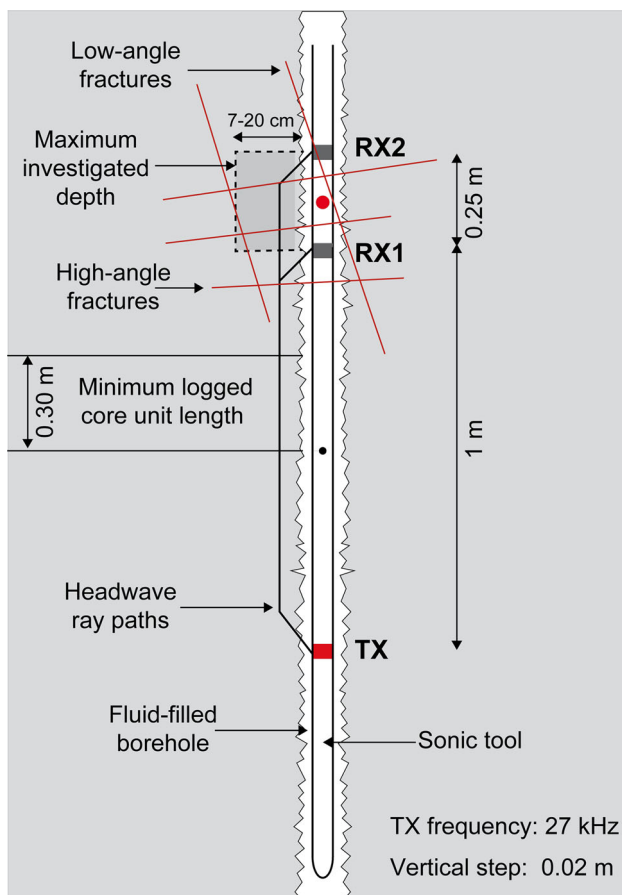


**Fig. 4** Operating scheme of the sonic tool used for borehole logging. Measurement depth refers to the middle point (red dot) between receivers RX1 and RX2. Receiver spacing (0.25 m) sets the vertical spatial resolution of the log. To ensure consistent averaging of localized effects, a minimum core unit length of 30 cm was considered in the geomechanical core logging. This is also convenient to account properly for the effect of discontinuity spacing on rock mass structure (color figure online)

Haldorsen et al. 2006). More recently, acoustic logging techniques were successfully applied to the geomechanical characterization of rock masses in boreholes (King et al. 1978; Moos and Zoback 1983; Jauch 2000). Acoustic energy emitted by piezoelectric transducers travels through the fluid used to couple the probe and the borehole wall and through the surrounding rock mass depending on its lithology, density, stiffness, weathering, porosity and fracturing. The travel times of transmitted (head) waves through the formation near the borehole wall or in the excavation damage zone (EDZ) allow evaluating the velocity of compressional (standard acoustic logs) or shear waves between receivers (Fig. 4).

In our study, the three boreholes were logged using a centered full-wave, two-receiver acoustic logging tool (SEMM Logging S.A.) with a diameter of 50 mm, a downhole source (TX) and two receivers spaced 1.0 (RX1) and 1.25 m (RX2) uphole the source, respectively

(Fig. 4). The tool was also equipped with two long-spacing receivers at 3.0 and 3.25 m, not used in our investigation. The transmitter operated at a frequency of 27 kHz, and the receivers recorded frequencies in the range 0–100 kHz. The travel times of acoustic P-waves and S-waves (some borehole segments only) were recorded in the 25-cm interval between RX1 and RX2, while raising the tool at a constant velocity of 1 cm/s with a 2-cm measurement step.

The receiver spacing sets the vertical resolution of the log (White 1962; King et al. 1978; Serra 1986; Franco et al. 2006; Haldorsen et al. 2006), which is thus in the order of 25 cm. This implies that the acoustic response of thinner layers, which may be faster or slower than the surrounding material, is averaged and smoothed, possibly resulting in local under- or overestimation of rock mass properties. The depth of penetration of refracted acoustic waves in the borehole surroundings is another critical issue when attempting an “equivalent continuum” characterization of fractured rock masses (King et al. 1978; Jauch 2000; Barton 2007). In fact, while full waveform analysis of acoustic logs allows characterizing individual fracture location and aperture (Brie et al. 1998; Franco et al. 2006; Haldorsen et al. 2006), the influence of individual discontinuities on the average velocity response of fractured media depends on their orientation and spacing with respect to the investigated volume around the borehole. The latter is independent on the receiver spacing, but depends on wavelength, which for a given transmitter frequency depends on formation velocity (in turn also depending on fracturing). In the studied case, with a source frequency of 27 kHz and in situ  $V_p$  values in a range 2000–5000 m/s, the depth of penetration ranges between 7 cm (slowest materials) and about 20 cm (fastest materials, Fig. 4). Therefore, in case of fracture spacing exceeding 30 cm, the recorded  $V_p$  will be basically approaching the intact rock  $V_p$ , depending on weathering and other secondary porosity effects (e.g., cavities).

A total length of 670 m of  $V_p$  logs was obtained for the three boreholes (location of logged segments in Fig. 3), at depths ranging between 100 and 400 m. Logging was not performed in some intervals of boreholes BH4 (185–223 m) and BH8 (340–350 m), due to borehole instability and risk of damage or loss of the logging equipment. In order to obtain a seismic dataset comparable with the geomechanical core log,  $V_p$  values recorded every 2 cm along the boreholes were averaged over 30-cm intervals. Both logs are plotted in Fig. 5.

The recorded dataset is characterized by a wide range of  $V_p$ , ranging between very low values (1700–1900 m/s) and values typical of intact rock (up to 5100–5300 m/s). These testify the extreme heterogeneity of the studied tectono-metamorphic sequence (Figs. 2, 3), representative of a

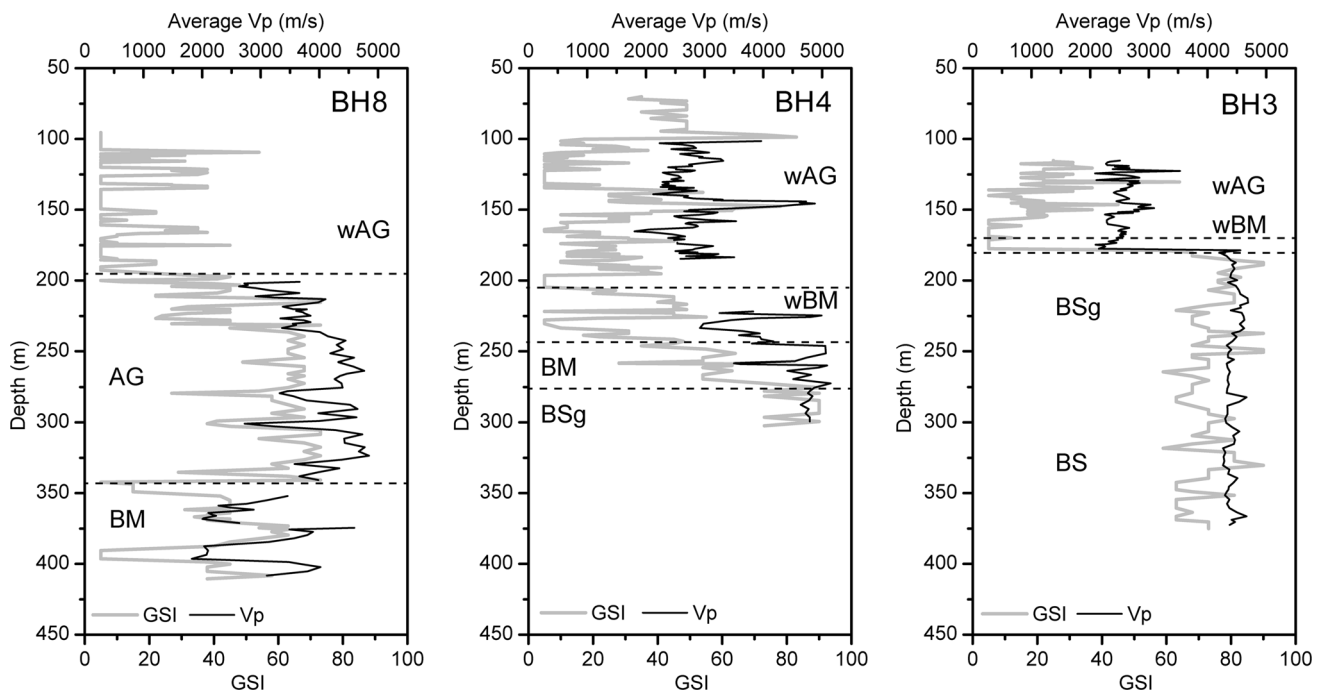


**Fig. 5** Logs of GSI (obtained for every core unit with minimum length 30 cm) and P-wave velocity ( $V_p$ , averaged over individual core units). Boundaries of main lithological units (Fig. 3) are indicated

wide range of lithological, geomechanical and depth conditions.

The weathered Antigorio gneiss (wAG), logged at shallow depths below the glacial deposits, shows  $V_p$  values generally ranging between 2200 and 3000 m/s. Nonetheless, the acoustic log effectively mirrored local heterogeneity by recording values lower than 2000 m/s in disintegrated gneiss layers, as well as values exceeding 4500 m/s where the boreholes crossed localized stretches of intact rock. In the BH8 borehole, the thick wedge of sound Antigorio gneiss encountered between 200 and 342 m in depth (below the DSGSD base and above the Baceno metasediments) is characterized by  $V_p$  values ranging between 3700 and 4700 m/s, with low-velocity stretches corresponding to damage zones of tectonic faults. The globally good quality of the AG rock mass is testified by the almost continuous recording of  $V_s$  values (not further considered here). At depth, the acoustic log mirrored the extreme heterogeneity of the Baceno metasedimentary sequence (BM). Here, marbles and calc-schist showed  $V_p$  values in the range 3000–4000 m/s, corresponding to the medium good rock mass quality directly observed in core logging. Conversely, in the two decomposed carbonate “sand” layers,  $V_p$  values lower than 2200 m/s were recorded (minimum about 1800 m/s). At depth, the occurrence of the high-quality basal anhydrite layer was testified in the acoustic log by high  $V_p$  values up to 5300 m/s. Finally, the Baceno mica schist (BS), encountered in the BH3 below 172.8 m and in the BH4 below

279 m in depth, is characterized by good and poorly variable rock mass quality, with  $V_p$  values ranging between 4500 and 5000 m/s, and by quite constant  $V_s$  values around 2500 m/s.

#### 4 Geological Strength Index Logging in Boreholes

To find correlations between the acoustic response of rock masses and their geomechanical quality at depth requires a versatile rock mass descriptor, to be derived from standard core logging information. To this aim, we used the Geological Strength Index (GSI). Initially proposed to support the parameterization of the Hoek–Brown failure criterion (Hoek et al. 1995, 2002; Hoek and Brown 1997), this rock mass description system turned out as an effective tool to account for rock mass structure and discontinuity conditions in difficult settings (Marinos and Hoek 2000; Marinos et al. 2005). These include weak (Hoek et al. 1998), lithologically heterogeneous (Hoek et al. 2005) or structurally complex rock masses (Marinos and Hoek 2001), as well as damaged rock masses in fault zones (Brideau et al. 2009) or rock slope instabilities (Agliardi et al. 2013).

In order to minimize subjectivity in GSI evaluation and overcome the scale-independent assessment of “blockiness” inherent in the GSI charts (Russo 2009), different multiparameter GSI quantification approaches were proposed according to a classical rock mass classification

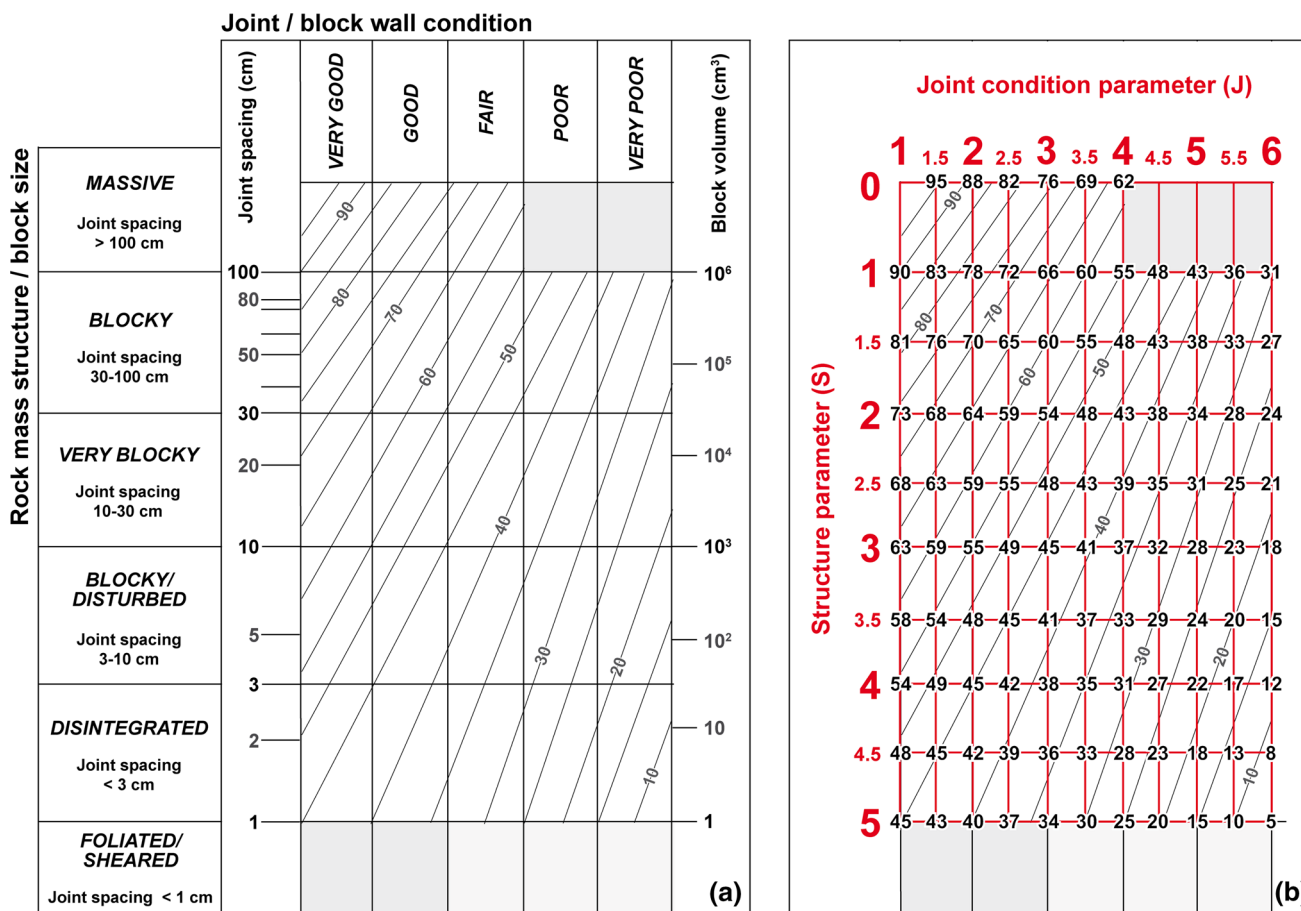


**Fig. 6** BH-GSI logging scheme, based on a unique-condition combination recoding of rock mass structure (parameter S, i.e., descriptors of fracture density in terms of total joints spacing or block volume)

and joint wall condition (parameter J, described in terms of weathering). GSI chart on the left is after Cai et al. (2004)

approach. They are usually based on empirical relationships between GSI variables (i.e., rock mass structures and discontinuity conditions) and quantitative descriptors used in other rock mass classification systems. Cai et al. (2004) proposed a modified GSI system (Fig. 6a) accounting for rock structure and joint conditions by introducing parameters proposed by Palmstrom (1996) in the framework of the Rmi system. Russo (2009) also proposed a method linking the GSI and Rmi approaches based on the formal similarity between the GSI and the joint parameter JP. Recently, Hoek et al. (2013) proposed a quantification of the GSI chart as a function of RQD and the joint conditions factors proposed by either Bieniawski (1989;  $J_{cond89}$ ) or Barton et al. (1974; Jr and Ja). Nevertheless, these approaches were developed for application on (natural or artificial) rock outcrops, which allow an effective geological evaluation of rock mass structure (i.e., degree of interlocking among rock blocks) and discontinuity conditions, including the number of joint sets, their geometry and persistence (i.e., block boundary conditions; Hoek and

Brown 1997). These parameters are difficult to evaluate in drill cores due to: (a) the limited extent of the investigated rock mass; (b) the 1D nature of borehole sampling and related biases; (c) the difficult identification of joint sets in non-oriented cores; and (d) the core diameter, limiting the observation of discontinuity geometry and size. In drill cores, rock mass structure description is thus limited to joint spacing or frequency (i.e., linear intensity,  $P_{10}$ ; Der-showitz and Herda 1992), and discontinuity conditions can be only described in terms of small-scale roughness and weathering. Nevertheless, Zhang (2016) evaluated the RQD evaluated from drill cores as a convenient parameter for estimating the mechanical properties of rock masses, and Lin et al. (2014) proposed a modification of the GSI system for application to drill cores in granitic rocks. Here, we propose a simple approach (BH-GSI) to evaluate the GSI from drill cores for application to a wide range of rock types (hard and weak metamorphic rocks, metasedimentary rocks) and structural conditions (sound/poorly fractured to weathered/disintegrated rock masses).



#### 4.1 BH-GSI Logging Method

We considered drill core runs as initial reference units for classification. Then, we obtained final classification “core units” by dividing core run segments with sharply different rock mass structure and grouping similar ones belonging to adjacent core runs. We considered a minimum core unit length of 30 cm in order to properly account for rock mass structure in low-quality rock masses (i.e., transition from “very blocky” to “blocky/disturbed”). Such minimum value is also consistent with the vertical resolution of sonic logs (Fig. 4). Core unit lengths ranged between 0.3 and 3.3 m, with mean values varying between 1.3 and 1.8 m in the different boreholes.

We classified individual core units by introducing two simple structure (S) and joint condition (J) parameters (Fig. 6; Table 2; intermediate values allowed), linked to the GSI scheme by Cai et al. (2004) and combined to obtain GSI borehole logs.

The structure parameter (S; Fig. 6b) is built on the assumption that reliable evidence of rock mass structure in drill cores is limited to joint spacing, although this is a biased measure of fracture abundance and block size. Since joint spacing is a continuous variable, we started from the GSI chart by Cai et al. (2004) and linked integer S values (up to 5) to the joint spacing (or block volume) values corresponding to the boundaries of Hoek and Brown rock mass types. We did not include in our system the “foliated/laminated/sheared” type of Hoek et al. (1998). In fact, foliations are major anisotropic fabric features of metamorphic rocks, which exert a stronger control on intact rock properties (Walsh and Brace 1964; Attewell and Sanford 1974; Agliardi et al. 2014) than on rock mass structure.

Regarding joint conditions, the joint condition factor proposed by Cai et al. (2004) appears unsuitable for application to drill cores. In fact, the limited exposure of discontinuities hampers the characterization of their large-scale waviness ( $J_w$ ), and it is nearly impossible to evaluate small-scale roughness (e.g., JRC, Barton et al. 1974) in highly fractured or weathered drill cores. At the same time, small-scale smoothness ( $J_s$ ) and alteration ( $J_a$ ) factors do not cover the range of joint conditions encountered in many cases (i.e., strongly weathered to disintegrated joint wall surfaces). Thus, assuming that weathering is the strongest indicator of joint conditions in drill cores, we adopted the discontinuity weathering description scheme proposed by ISRM (1978; Table 2). The latter has three practical advantages: (a) it covers a broad range of conditions, from clean rock joints to decomposed joint walls; (b) it is consistent with the joint condition descriptions of the original GSI charts (Hoek and Brown 1997; Marinos and Hoek 2000); (c) it is commonly used in standard geomechanical core logging directly at drilling sites. Our joint condition parameter J (Fig. 6b) depends on ISRM weathering conditions and has integer values (1–6) fitting the boundaries of Hoek and Brown joint condition categories.

In the BH-GSI method, values of S and J are attributed to each core unit to estimate the GSI according to a “unique-condition” approach (Fig. 6): each S–J (non-commutative) combination corresponds to a unique GSI value sampled from the GSI chart of Cai et al. (2004; Fig. 6a) using a grid overlay (Fig. 6b). The procedure was applied to 515 core units of the three studied boreholes, for a total core length of 812 m. Resulting GSI logs are plotted in Fig. 5 with the corresponding  $V_p$  logs.

In order to check the general consistency of the method, we compared the estimated BH-GSI values to those

**Table 2** Keys to structure and joint condition parameters in the BH-GSI logging scheme

Structure parameter (S)	Description (total spacing)
0	>1 m: “massive” rock
1	1 m: lower limit of “massive” rock
2	0.3 m: “blocky” to “very blocky” transition
3	0.1 m: “very blocky” to “disturbed” transition
4	0.03 m: “disturbed” to “disintegrated” transition
5	0.01 m: upper limit of soil-like material
Joint condition parameter (J)	Description (weathering)
1	Fresh, unweathered surfaces
2	Slightly weathered, discolored surfaces
3	Moderately weathered surfaces, staining
4	Highly weathered surfaces, coatings
5	Highly weathered, decomposed surfaces, fillings
6	Completely decomposed surface material

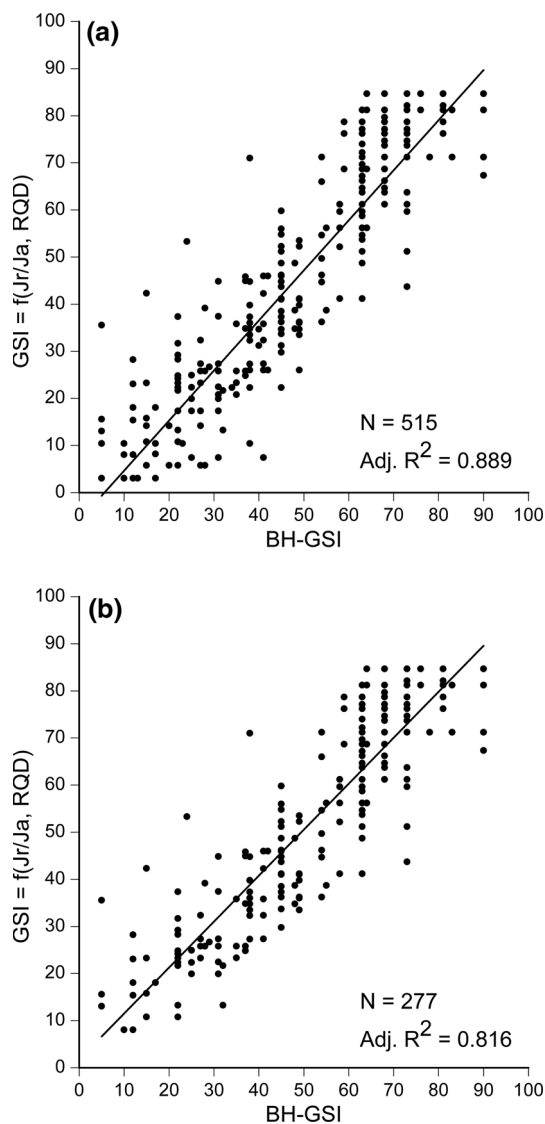


**Fig. 7** Comparison of GSI values calculated using the BH-GSI method and the quantification method by Hoek et al. (2013). See text for explanation. **a** Linear fit including the entire core unit dataset; **b** linear fit performed excluding core units characterized by RQD = 0

obtained using a GSI quantification method proposed by Hoek et al. (2013). We use their empirical formula relating GSI to the Jr/Ja ratio (Barton et al. 1974) and RQD:

$$\text{GSI} = \frac{52(\text{Jr}/\text{Ja})}{1 + (\text{Jr}/\text{Ja})} + \frac{\text{RQD}}{2} \quad (1)$$

where parameters Jr, Ja and RQD were derived for each core unit following standard procedures (Deere 1963; Barton et al. 1974).

BH-GSI values show a reasonably good linear correlation to the GSI values quantified according to Hoek et al. (2013). Including GSI data quantified from core units with RQD = 0 maximizes the least-square goodness of fit (Fig. 7a), but results in underestimated “quantified” GSI

with respect to BH-GSI, due to the inability of the RQD to properly account for fracture intensity in poor-quality rock masses. This effect vanishes if the RQD = 0 core unit data (indeed representing 50 % of the dataset) are excluded (Fig. 7b). Although RQD is also insensitive to changes in quality of very good rock masses (RQD = 100), we suggest that the good correlation between BH-GSI and the “quantified” GSI (Hoek et al. 2013) for high-quality rock masses depends on the contribution of the joint alteration number (Ja), which decreases with increasing rock mass quality. The comparison suggests that the BH-GSI procedure provides consistent results in a wide range of rock masses, characterized by contrasting rock types, fracture intensity and weathering conditions.

## 4.2 BH-GSI Logging Results

The GSI logs obtained using the BH-GSI approach provide a very satisfactory account of the geological and geomechanical complexity directly observed in the boreholes and indirectly detected by acoustic logging (Figs. 3, 5, 8).

The two observed rock mass “facies” of the Antigorio gneiss are mirrored by distinct GSI value populations. The intensely fractured and weathered facies (wAG) is characterized by average GSI in the range 15–25, maximum values up to 83 in less fractured portions, and highest values and heterogeneity in the borehole BH4 (Fig. 3). The “sound” facies (AG) found in the borehole BH8 is characterized by average GSI value of 55 and maximum values reaching 75, due to low fracture intensity and very low degree of weathering (Fig. 8a). The underlying Baceno metasediments (BM) are characterized by highly variable GSI, with global average values in the range 38–58 (depending on the considered borehole) and typical values of 5–15 for carbonate sand layers (Fig. 8b), 45–65 for fractured calc-schist (Fig. 8c), 65–70 for sound marble layers and 75–90 in the high-quality basal anhydrite layer in the borehole BH4 (Fig. 8d). Finally, the Baceno mica schist (BSg and BS) is characterized by high GSI values (average 75–85, maximum 90) and low vertical variability.

## 5 Vp–GSI Relationships

The clear qualitative correlation between Vp and GSI logs (Fig. 5) motivated the search for quantitative relationships linking the acoustic response of rock masses to their geomechanical quality for practical applications. We identified candidate empirical correlation functions using a two-step statistical analysis procedure, involving: (1) preliminary identification and removal of statistical outliers; (2) curve fitting by linear and nonlinear regression techniques.

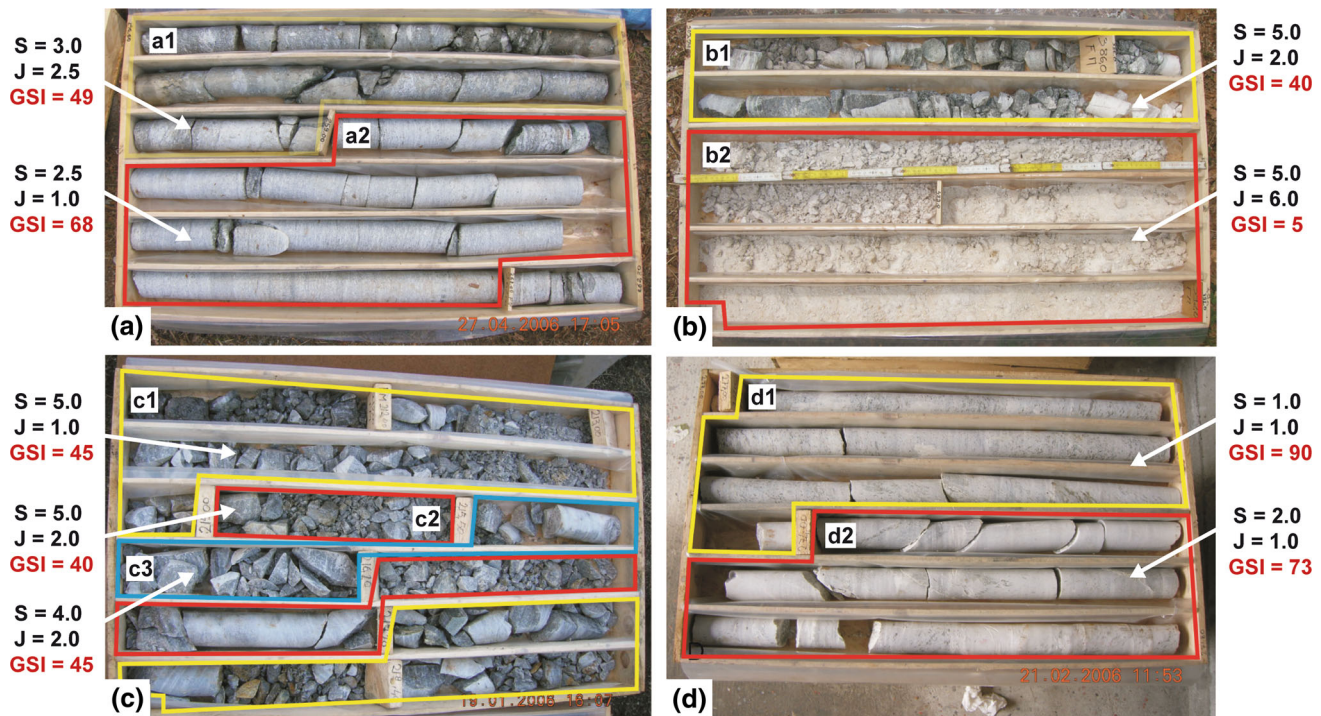


**Fig. 8** Examples of BH-GSI classification of core units in the main rock types found in the studied boreholes (locations in Fig. 3). **a** Borehole BH8: Antigorite gneiss (AG) of average quality (GSI = 49, unit a1) and good quality (GSI = 68, unit a2), respectively; **b** borehole BH8: fractured BM marble layers (GSI = 40, unit

b1) and carbonate sands derived from the complete degradation of marble (GSI = 5, unit b2); **c** borehole BH4: fractured calc-schist and dolomitic marble layers (BM); **d** borehole BH4: anhydrite layers (BM) with very low degree of fracturing and alteration, mirrored by high P-wave values in the sonic logs

### 5.1 Outlier Filtering

Our dataset consists of 364  $V_p$ –GSI data pairs (Fig. 9a), corresponding to the core units for which both  $V_p$  and GSI logs are available (Figs. 3, 5). The dataset is characterized by a significant scattering, consistent with the extreme variability of encountered rock types, structural conditions, weathering and joint conditions. Thus, in order to attempt a robust statistical regression analysis, it was necessary to perform a preliminary identification and filtering of statistical outliers, i.e., data pairs presumed to come from different distributions than that accounting for most of the dataset (Schwertman et al. 2004). In our dataset, outliers were likely related to geophysical measurement errors, local core logging inaccuracies and the extremely high natural variability of rock mass properties, due to the very different observed combinations of fracture intensity and weathering. We identified outliers using a graphical boxplot method commonly used in exploratory data analysis (Tukey 1977; Frigge et al. 1989; Schwertman et al. 2004). In particular, we used the “fences” procedure based on the interquartile range (IQR, i.e., the difference between the 3rd and 1st quartiles of the population), which provides a measure of data dispersion unaffected by potential extreme outliers (Tukey 1977). We subdivided the dataset into bins

every GSI = 5 and created boxplots to explore the distributions of  $V_p$  values falling into each bin (Fig. 9b). The adopted bin size proved to be a reasonable compromise between bin data numerosity and consistency between  $V_p$  values and the rock mass conditions (GSI) they refer to. We considered as outliers all the data points falling above the upper inner fence (UIF = 3rd Quartile + 1.5 IQR) and below the lower inner fence (LIF = 1st Quartile – 1.5 IQR), including both the “outside” and “far out” outliers of Tukey (1977).

Points classified as outliers were further checked, and those related to clear core logging errors were corrected. Our analysis resulted in the identification of 86 outliers, representing 23 % of the entire datasets. Such a large number of outliers is reasonable due to the conservative approach used and the very high variability of rock mass conditions described by acoustic logging. We excluded data pairs classified as outliers (red dots in Fig. 9) from further analysis.

### 5.2 Curve Fitting

The remaining 278 data pairs were fitted by nonlinear regression techniques based on Chi-Square minimization algorithms including Levenberg–Marquardt and downhill

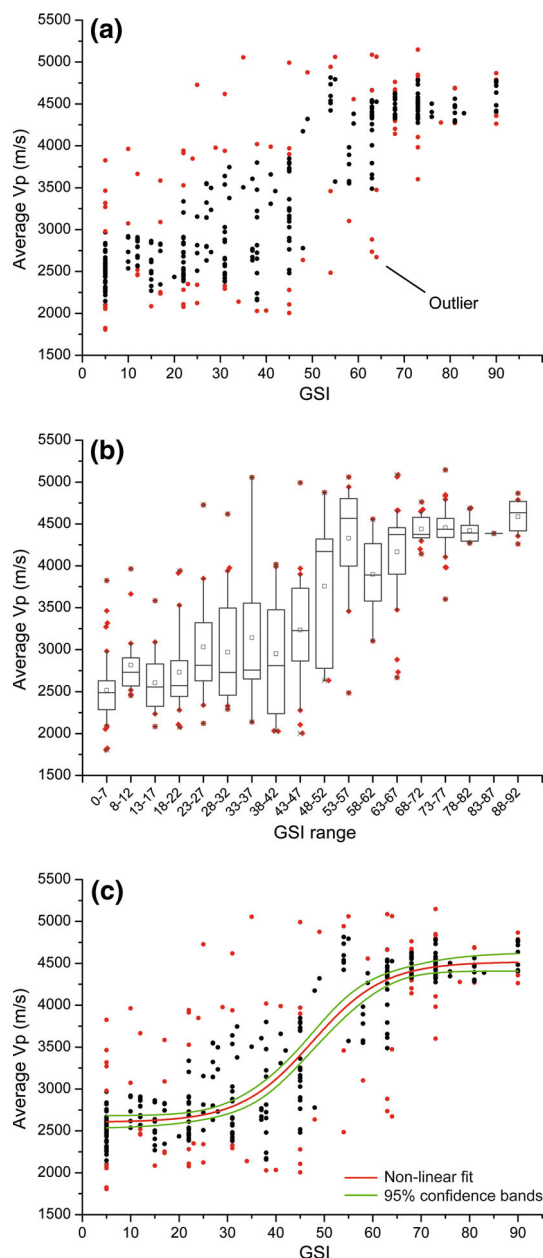


**Fig. 9** Identification and filtering of statistical outliers in the  $V_p$ -GSI dataset (364 data pairs). **a**  $V_p$ -GSI scatterplot (red dots: outliers); **b** outlier identification by boxplots representing P-wave velocity distributions for different GSI value ranges (whisker lengths correspond to upper and lower “inner fences” based on interquartile range, IQR; upper inner fence = 3rd quartile + 1.5\* IQR; lower inner fence = 1st quartile - 1.5\* IQR); **c** nonlinear curve fitting (Boltzmann sigmoidal fit)

simplex approximations (Bates and Watts 1988; Draper and Smith 1998).

We tested different candidate regression functions, including a simple linear function and two sigmoid functions (i.e., Boltzmann and Logistic). The latter are commonly used to describe “dose–response” systems with asymptotic behavior. Following the approach of most

literature studies (see Sect. 1), we selected the rock mass quality descriptor (GSI) as the independent variable and the related geophysical response ( $V_p$ ) as the dependent one.

We evaluated the suitability of the different regression models by analyzing residuals to check for independence of the error terms, normality of variance and absence of process drifts. We then evaluated the goodness of fit of different regression models in terms of adjusted coefficient of determination ( $R^2$ ) and root-mean-square errors (Table 3).

Although all tested regression models provided a statistically acceptable description of the dataset, the linear one resulted the less performing, with low fit quality and some variable error dependence and drift. In particular, the linear model does not account for very low and very high values of GSI and was discarded. Sigmoid functions provided the best fitting performance for the entire dataset (Figs. 9, 10; Table 3). We adopted the Boltzmann model in the form of the following empirical equation:

$$V_p(\text{m/s}) = 4520 - \frac{1920}{1 + e^{(\text{GSI}-47.5)/7.4}} \quad (2)$$

Equation 2 provides the best fit of the data over the full range of GSI and effectively accounts for the observed asymptotic behavior, with two distinct “plateaus” for very low (<20–25) and high (>65) GSI values (Fig. 10). The lower plateau likely describes the asymptotic P-wave velocity of disintegrated and highly weathered material. On the contrary, the upper plateau is intrinsically related to the acoustic logging technology, which limits the investigation depth to about 20 cm (Fig. 4). In rock masses with  $\text{GSI} > 65$  (i.e., fracture spacing exceeding values of 30–100 cm depending on fracture conditions), this results in record P-wave velocities approaching the limiting one of intact rock. Trying to fit the subset of data characterized by  $\text{GSI} < 65$  (i.e., upper plateau removed) using linear, exponential or sigmoidal functions does not give better results (Table 3).

## 6 Discussion and Conclusions

Statistically sound correlations between rock mass quality descriptors and the corresponding geophysical response (e.g., P-wave velocity) are useful tools in underground engineering, reservoir characterization or large slope instability studies. They allow obtaining cost-effective, preliminary estimates of the strength, deformability and permeability of rock masses with different structural complexity, forming large geological domains up to great depths (Barton 2002). These estimates are based on surface geophysical methods, geophysical borehole logging or their combinations and allow limiting the number of full-

**Table 3** Summary of regression statistics for different Vp–GSI curve fitting models.

	<i>N</i>	DoF	Adj. <i>R</i> <sup>2</sup>	RMSE
<b>Boltzmann sigmoid model, full GSI range</b>	<b>278</b>	<b>274</b>	<b>0.855</b>	<b>330</b>
Logistic sigmoid model, full GSI range	278	274	0.852	333
Linear model, full GSI range	278	276	0.811	377
Logistic sigmoid model, GSI < 65	206	202	0.722	377
Exponential model, GSI < 65	206	203	0.721	378
Linear model, GSI < 65	206	204	0.662	416

Bold values indicate best-fitting model (Equation 2)

See text for discussion

*N* number of considered data points, *DoF* degrees of freedom, *Adj. R*<sup>2</sup> adjusted *R*<sup>2</sup> (corrected for DoF), *RMSE* root-mean-square error, in m/s

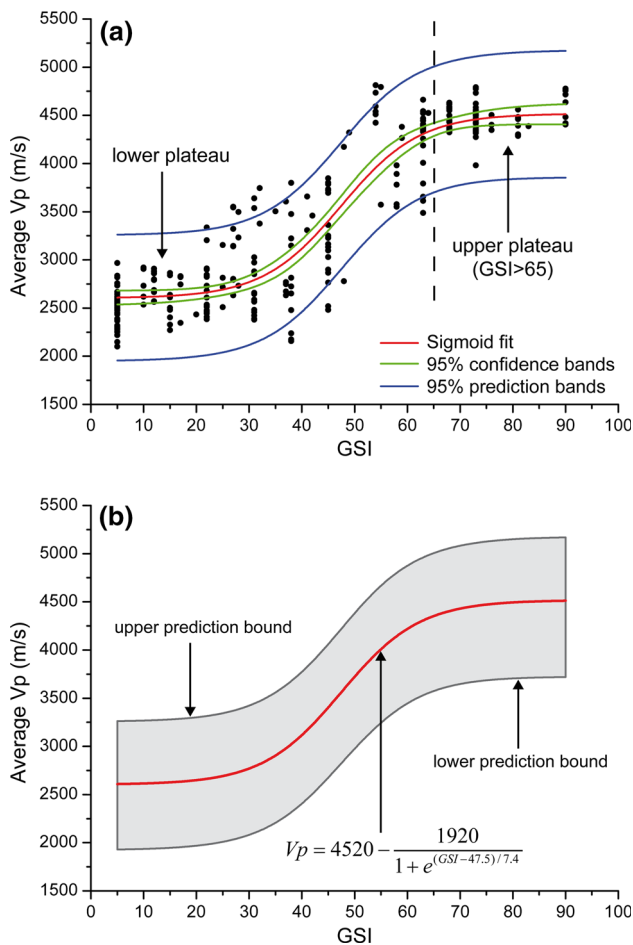


**Fig. 10** Empirical Vp–GSI relationship derived by nonlinear statistical regression analysis. **a** Plot of the best fitting regression function for the entire outlier-free dataset. Confidence and prediction bands for the 95 % confidence level are outlined. **b** Proposed empirical function and associated predictive capability and error (gray area is the prediction range for the 95 % confidence level, i.e., the area in which 95 % of the experimental points are expected to fall

core boreholes (and related core logging activities) to that required to calibrate geophysical datasets.

Existing correlations between Vp and rock mass quality descriptors as RQD (Deere et al. 1967; Sjøgren et al. 1979;

Palmström 1995, 1996) or Q (Barton 1991, 1995) are consistently applicable only at very shallow depths (up to few tens of meters) and in relatively homogeneous hard rocks (Barton 2007). Moreover, the applicability of more complex relationships accounting for the effects of depth or porosity (Barton 1995, 2002, 2007) can be limited by the lack of site-specific validation data and by the unclear dependence of Vp on depth. This is the case of our dataset, in which no defined Vp–depth trends occur, in agreement with the results obtained by Moos and Zoback (1983) in irregularly fractured rocks.

Our work resulted in a versatile empirical relationship between Vp and GSI (Fig. 10), accounting for the geophysical responses of very different rock type, structural and weathering conditions over a depth range between 100 and 400 m. Since no shallow data (<100 m) were considered, our empirical function is not affected by very shallow-depth effects (Cecil 1971; Sjøgren et al. 1979; Barton 2007) and can be considered as complementing previously published ones. Over the investigated depth range, a complex dependence of Vp on fracture abundance and rock mass quality derived by core logging is evident. Consistently with Moos and Zoback (1983), we observed Vp values poorly varying with depth in borehole stretches in high-quality rock masses (e.g., Baceno mica schist in BH3) and Vp values often increasing with depth in heavily fractured rock masses (e.g., top of sound Antigorio gneiss AG in BH8; Baceno metasediments in BH4). In any case, the dependence of Vp (locally measured by sonic logging) on rock mass quality (locally evaluated by direct core logging) is consistently captured by our empirical relationship over the entire considered depth range, which is quite significant considering engineering applications. We do not propose any generalization of our results at deeper levels, but suggest that they may apply upon experimental validation.

The use of acoustic (sonic) borehole logging techniques has the advantage to overcome some limitations of surface seismic refraction techniques and allows a direct comparison with geomechanical core logging at each depth level.

Moreover, using the GSI to describe rock mass conditions in drill cores has several advantages: (1) it is suitable for application to almost all types of rock masses, from massive to disintegrated and strongly weathered, with different degrees of structural complexity; (2) it can be easily quantified during standard geomechanical logging of high-quality drill cores using the proposed BH-GSI procedure; (3) it is by definition independent on water content and boundary stress state; (4) it provides a direct input to the parameterization of rock mass strength and deformability via the Hoek–Brown approach.

Since the BH-GSI is estimated from borehole data, its structure parameter ( $S$ ) chiefly depends on total joint spacing. Thus, it is by definition affected by orientation and size biases typical of every kind of 1D sampling. Nevertheless, these biases also affect geophysical borehole logging and do not hamper the consistency of the empirical correlation analysis. In addition, the joint condition parameter ( $J$ ) mainly depends on weathering, because a reliable estimate of small-scale roughness is difficult or impossible to obtain in drill cores of variable quality. Nonetheless, on engineering problem scales, roughness is expected to have a minor influence on the properties of both low-GSI rock masses (i.e., small, poorly interlocked blocks) and high-GSI rock masses (i.e., large blocks in contact, reduced roughness due to the effect of scale; see Bandis et al. 1981). On the other hand, core logging evidence suggests that weathering accounts for geophysical response much more than roughness.

The sigmoid (asymptotic) form of the proposed empirical  $V_p$ –GSI function is consistent with statistical fitting performance and observed physical and technological constraints (Fig. 10a). The “lower plateau” ( $GSI < 25$ ) accounts for the geophysical response of the transition between fractured rock masses (Fig. 8a) and saturated granular, soil-like disintegrated rock masses (Fig. 8b). Similar conditions were not considered in the datasets on which previously published empirical relationships were built (Barton 2007). On the other hand, the “upper plateau” ( $GSI > 65$ ) is similar to what was observed by King et al. (1978) when characterizing fracturing of relatively sound andesite by borehole acoustic logging. As suggested in Sect. 5, we interpret the upper plateau as an effect of the limited volume investigated by sonic logging: In fact, in high-quality rock masses, spaced fractures have a reduced influence on the  $V_p$  recorded in the borehole surrounding, which approaches values typical of intact rock. Notwithstanding this limitation, the sigmoid function proved effective in discriminate rock mass quality for intermediate GSI values, where small changes can correspond to significantly different rock mass performances and costs in engineering applications.

In order to provide a versatile engineering tool for practical applications, we included the raw dataset (Figs. 9, 10a) and an analysis of errors and their impacts on the predictive capabilities of the empirical relationship (Fig. 10b). The high number of  $V_p$ –GSI data pairs classified as outliers (up to 23 % of the dataset) is consistent with the spatial resolution of the acoustic logging, which can be influenced by narrow fractured zones, intact layers or individual open persistent fractures. Outliers were filtered using a standard, conservative statistical approach in order to improve the quality of regression analysis. Nevertheless, a practical user will still need to be aware of the errors associated with “best-fit” proposed empirical functions when evaluating their performance in real case studies. This is particularly important when attempting to recognize and filter outlier rock mass properties in real-world applications. Thus, we provided prediction bands for a 95 % confidence level, i.e., the distances from the best-fit equation in which 95 % of experimental points are expected to fall. When attempting to predict GSI from sonic  $V_p$  in practical applications, experimental data outside the prediction band (Fig. 10b) should be treated with care (if close to the prediction bounds) or discarded as outliers (if far from them). Of course, this applies in lithological and depth settings similar to those in which we derived our empirical function, indeed quite broad. In this form, our empirical relationship has a potential for application to characterize rock mass strength and deformability in a variety of geological and geomechanical settings at depth, provided that: (1) site-specific calibration/validation is performed using few full-core borehole information; (2) prediction uncertainty is explicitly considered.

**Acknowledgments** We thank ENEL S.p.A. and the personnel of the Crevoladossola facility for providing access to core boxes and to the site investigation data. We are grateful to Alberto Villa for sharing interesting discussions on acoustic logging interpretation.

## References

- Agliardi F, Crosta GB, Zanchi A (2001) Structural constraints on deep-seated slope deformation kinematics. *Eng Geol* 59:83–102
- Agliardi F, Crosta GB, Frattini P (2012) Slow rock slope deformation. In: Clague JJ, Stead D (eds) *Landslides: types, mechanisms and modelling*. Cambridge University Press, Cambridge, pp 207–221
- Agliardi F, Crosta GB, Meloni F, Valle C, Rivolta C (2013) Structurally-controlled instability, damage and slope failure in a porphyry rock mass. *Tectonophysics* 605:34–47
- Agliardi F, Zanchetta S, Crosta GB (2014) Fabric controls on the brittle failure of folded gneiss and schist. *Tectonophysics* 637:150–162
- Albert W (2000) Petrophysical parameters—an indication of rock permeability? *Nagra Bull* 26:26–37

- ASTM Standard D2845-08 (2008) Standard test method for laboratory determination of pulse velocities and ultrasonic elastic constants of rock. ASTM International, West Conshohocken. [www.astm.org](http://www.astm.org)
- Attewell PB, Sanford MR (1974) Intrinsic shear strength of brittle anisotropic rock-I: experimental and mechanical interpretation. *Int J Rock Mech Min Sci* 11:423–430
- Bandis S, Lumsden AC, Barton NR (1981) Experimental studies of scale effects on the shear behaviour of rock joints. *Int J Rock Mech Min Sci* 18(1):1–21
- Barton N (1991) Geotechnical design. *World Tunnelling*, November 1991, pp 410–416
- Barton N (1995) The influence of joint properties in modelling jointed rock masses. Keynote lecture. In: Fuji T (ed) Proceedings of 8th ISRM congress, Tokyo, vol 3. Balkema, Rotterdam, pp 1023–1032
- Barton N (2002) Some new Q-value correlations to assist in site characterisation and tunnel design. *Int J Rock Mech Min Sci* 39:185–216
- Barton N (2007) Rock quality, seismic velocity, attenuation and anisotropy. Taylor & Francis, London
- Barton N, Lien R, Lunde J (1974) Engineering classification of rock masses for the design of tunnel support. *Rock Mech* 6(4):189–236
- Bates DM, Watts DG (1988) Nonlinear regression analysis & its applications. Wiley, New York
- Bieniawski ZT (1989) Engineering rock mass classifications: a complete manual for engineers and geologists in mining, civil, and petroleum engineering. Wiley, New York
- Bigoggero B, Boriani A, Giobbi E (1977) Microstructure and mineralogy of an orthogneiss (Antigorio gneiss-Lepontine Alps). *Rend Soc It Min Petr* 33:99–108
- Brideau M-A, Yan M, Stead D (2009) The role of tectonic damage and brittle rock fracture in the development of large rock slope failures. *Geomorphology* 103:30–49
- Brie A, Endo T, Hoyle D, Codazzi D, Esmersoy C, Hsu K, Sinha B (1998) New directions in sonic logging. *Oilfield Rev* 10(1):40–55
- Cai M, Kaiser PK, Uno H, Tasaka Y, Minami M (2004) Estimation of rock mass deformation modulus and strength of jointed hard rock masses using the GSI system. *Int J Rock Mech Min Sci* 41:3–19
- Campani M, Mancktelow N, Seward D, Rolland Y, Müller W, Guerra I (2010) Geochronological evidence for continuous exhumation through the ductile-brittle transition along a crustal-scale low-angle normal fault: Simplon Fault Zone, central Alps. *Tectonics*. doi:10.1029/2009TC002582
- Cecil OS (1971) Correlation of seismic refraction velocities and rock support requirements in Swedish tunnels. *Statens Geotekniska Institut. Publ*, vol 40
- Deere DU (1963) Technical description of rock cores for engineering purposes. *Felsmechanik und Ingenieurgeologie* 1(1):16–22
- Deere DU, Jr AJ Hendron, Patton FD, Cording EJ (1967) Design of surface and near surface construction in rock. In: Fairhurst C (ed) Failure and breakage of rock, 237302. Society of Mining Engineers of AIME, New York
- Dershowitz WS, Herda HH (1992) Interpretation of fracture spacing and intensity. In: The 33th US symposium on rock mechanics (USRMS). American Rock Mechanics Association
- Draper NR, Smith H (1998) Applied regression analysis, 3rd edn. Wiley, New York
- Franco JA, Ortiz MM, De GS, Renlie L, Williams S (2006) Sonic investigation in and around the borehole. *Oilfield Rev* 18(1):14–31
- Frigge M, Hoaglin DC, Iglewicz B (1989) Some implementations of the boxplot. *Am Stat* 43(1):50–54
- Gong G (2005) Physical properties of alpine rocks: a laboratory investigation. Dissertation, Thèse de doctorat, Univ. Genève, no. Sc. 3658
- Grasemann B, Mancktelow N (1993) Two-dimensional thermal modelling of normal faulting: the Simplon Fault Zone, Central Alps, Switzerland. *Tectonophysics* 225:155–165
- Griffiths DH, King RF (1987) Geophysical exploration. In: Bell FG (ed) Ground engineers reference book. Butterworths, London, pp 27/1–27/21
- Haldorsen JB, Johnson DL, Plona T, Sinha B, Valero HP, Winkler K (2006) Borehole acoustic waves. *Oilfield Rev* 18(1):34–43
- Hoek E, Brown ET (1997) Practical estimates of rock mass strength. *Int J Rock Mech Min Sci* 34(8):1165–1186
- Hoek E, Kaiser PK, Bawden WF (1995) Support of underground excavations in hard rock. Balkema, Rotterdam
- Hoek E, Marinos P, Benissi M (1998) Applicability of the Geological Strength Index (GSI) classification for very weak and sheared rock masses. The case of the Athens Schist Formation. *Bull Eng Geol Env* 57(2):151–160
- Hoek E, Carranza-Torres C, Corkum B (2002) Hoek-Brown failure criterion—2002 edition. In: Proceedings North American Rock Mechanics Society, Toronto, July 2002
- Hoek E, Marinos PG, Marinos VP (2005) Characterisation and engineering properties of tectonically undisturbed but lithologically varied sedimentary rock masses. *Int J Rock Mech Min Sci* 42:277–285
- Hoek E, Carter TG, Diederichs MS (2013) Quantification of the Geological Strength Index Chart. In: 47th US rock mechanics/geomechanics symposium. American Rock Mechanics Association, paper 13-672
- Hudson JA, Jones EJW, New BM (1980) P-wave velocity measurements in a machine-bored, chalk tunnel. *Q J En Geol* 13:33–43
- International Society of Rock Mechanics (1978) Suggested methods for the quantitative description of discontinuities in rock masses. *Int J Rock Mech Min Sci Geomech Abst* 15:319–368
- Jauch F (2000) Using borehole geophysics for geotechnical classifications of crystalline rock masses in tunnelling. Dissertation, ETH PhD Thesis no. 13663
- Jorden JR, Campbell FL (1986) Well logging II—electric and acoustic logging, vol 10. SPE Monograph Series, pp 95–151
- King MS (2009) Recent developments in seismic rock physics. *Int J Rock Mech Min Sci* 46(8):1341–1348
- King MS, Stauffer MR, Pandit BI (1978) Quality of rock masses by acoustic borehole logging. In: Proceedings 3rd international congress IAEG, Madrid, section IV, 1, pp 156–164
- Lin D, Sun Y, Zhang W, Yuan R, He W, Wang B, Shang Y (2014) Modifications to the GSI for granite in drilling. *Bull Eng Geol Env* 73(4):1245–1258
- Mancktelow NS (1985) The Simplon Line: a major displacement zone in the Western Lepontine Alps. *Eclogae Geol Helv* 78:73–96
- Marinos P, Hoek E (2000) GSI: a geologically friendly tool for rock mass strength estimation. In: ISRM international symposium. International Society for Rock Mechanics
- Marinos P, Hoek E (2001) Estimating the geotechnical properties of heterogeneous rock masses such as Flysch. *Bull Eng Geol Env* 60:85–92
- Marinos V, Marinos P, Hoek E (2005) The geological strength index: applications and limitations. *Bull Eng Geol Env* 64(1):55–65
- Mavko G, Mukerji T, Dvorkin J (1998) The rock physics handbook: tools for seismic analysis in porous media. Cambridge University Press, Cambridge
- Maxelon M, Mancktelow NS (2005) Three-dimensional geometry and tectonostratigraphy of the Pennine zone, Central Alps, Switzerland and Northern Italy. *Earth Sci Rev* 71:171–227

- McDowell PW (1993) Seismic investigation for rock engineering. *Comprehensive Rock Engineering*, vol 3, Rock testing and site characterization. Oxford, Pergamon, pp 619–634
- Milnes AG, Grellier M, Muller R (1981) Sequence and style of major post-nappe structures, Simplon-Pennine Alps. *J Struct Geol* 3(4):411–420
- Moos D, Zoback MD (1983) In-situ studies of velocities in fractured crystalline rocks. *J Geophys Res* 88(B3):2345–2358
- New BM, West G (1980) The transmission of compressional waves in jointed rock. *Eng Geol* 15:151–161
- Nur A, Mavko G, Dvorkin J, Galmudi D (1998) Critical porosity: a key to relating physical properties to porosity in rocks. *Lead Edge* 17(3):357–362
- Palmstrom A (1996) Application of seismic refraction survey in assessment of jointing. In: Conference on recent advances in tunnelling technology, New Delhi
- Palmstrom A (2005) Measurements of and correlations between block size and rock quality designation (RQD). *Tunn Undergr Space Technol* 20(4):362–377
- Palmström A (1995) RMI—a rock mass characterization system for rock engineering purposes. Dissertation, Ph.D thesis, University of Oslo, Norway
- Press F (1966) Seismic velocities. *Handbook of physical constants*. In: Clark SG (ed) Geological Society of America, pp 195–218
- Russo G (2009) A new rational method for calculating the GSI. *Tunn Undergr Space Technol* 24(1):103–111
- Sapigni M, Baldi AM, Bianchi F, De Luca J (2012) High-resolution multichannel seismic survey for the excavation of the new headrace tunnel for the Crevola Toce III Hydropower scheme in the Ossola Valley, Italy. *Geotechnical Aspects of Underground Construction in Soft Ground*, p 137
- Schwertman NC, Owens MA, Adnan R (2004) A simple more general boxplot method for identifying outliers. *Comput Stat Data Anal* 47(1):65–174
- Serra O (1986) *Fundamentals of well-log interpretation (vol. 2): the interpretation of logging data (developments in petroleum science)*. Elsevier, Amsterdam
- Sjøgren B (1984) *Shallow refraction seismics*. Chapman & Hall, London
- Sjøgren B, Øvsthus A, Sandberg J (1979) Seismic classification of rock mass qualities. *Geophys Prospect* 27(2):409–442
- Stacey TR (1977) Seismic assessment of rock masses. In: Symposium on exploration for rock engineering, Johannesburg 1976, vol 2, Balkema, Rotterdam, pp 113–117
- Steck A (2008) Tectonics of the Simplon massif and Lepontine gneiss dome: deformation structures due to collision between the underthrusting European plate and the Adriatic indenter. *Swiss J Geosci* 101(2):515–546
- Steck A, Della Torre F, Keller F, Pfeifer H-R, Hunziker J, Masson H (2013) Tectonics of the Lepontine Alps: ductile thrusting and folding in the deepest tectonic levels of the Central Alps. *Swiss J Geosci* 106:427–450
- Tukey JW (1977) *Exploratory data analysis*. Addison-Wesley, Reading
- Walsh JB, Brace WF (1964) A fracture criterion for brittle anisotropic rock. *J Geophys Res* 69:3449–3456
- Watkins JS, Walters LA, Godson RH (1972) Dependence of in situ compressional wave velocity on porosity in unsaturated rocks. *Geophysics* 37:29–35
- Westerman AR, Reeves MJ, Attwell PB (1982) Rock surface roughness and discontinuity closure at depth. *Developments in Geotechnical Engineering*, vol 32. Elsevier, Amsterdam, pp 63–67
- White JE (1962) Elastic waves along a cylindrical bore. *Geophysics* 27:327–333
- White JE (1967) The hula log: a proposed acoustic tool. In: *Translations of SPWLA, 8th annual logging symposium*, paper I
- Zhang L (2016) Determination and applications of rock quality designation (RQD). *J Rock Mech Geotech Eng* 8(3):389–397